Letter

Sensitivity of the MnTe valence band to the orientation of magnetic moments

Paulo E. Faria Junior,[1] Koen A. de Mare,[2,3] Klaus Zollner,[1] Kyo-hoon Ahn,[3] Sigurdur I. Erlingsson,[4] Mark van Schilfgaarde,[5,6] and Karel Výborný[3]

[1]*Institute for Theoretical Physics, University of Regensburg, D-93040 Regensburg, Germany*
[2]*Eindhoven University of Technology, Eindhoven NL-5612 AZ, Netherlands*
[3]*FZU-Institute of Physics of the Czech Academy of Sciences, Cukrovarnická 10, Praha CZ-16253, Czech Republic*
[4]*Department of Engineering, School of Technology, Reykjavik University, Menntavegi 1, IS-102 Reykjavik, Iceland*
[5]*National Renewable Energy Laboratory, Golden, Colorado 80401, USA*
[6]*Department of Physics, King's College London, Strand, London WC2R 2LS, United Kingdom*

(Received 23 September 2022; accepted 8 February 2023; published 27 March 2023)

An effective model of the hexagonal (NiAs-structure) manganese telluride valence band in the vicinity of the A point of the Brillouin zone is derived. It is shown that whereas for the usual antiferromagnetic order (magnetic moments on the basal plane) band splitting at A is small, their out-of-plane rotation enhances the splitting dramatically (to about 0.5 eV). We propose extensions of recent experiments [Phys. Rev. Mater. **6**, 014404 (2022)] where such inversion of magnetocrystalline anisotropy has been observed in Li-doped MnTe to confirm this unusual sensitivity of a semiconductor band structure to magnetic order.

DOI: 10.1103/PhysRevB.107.L100417

I. Introduction. The electronic structure of crystalline semiconductors can be treated by various methods, which differ greatly in their computational cost [1]. Among *ab initio* methods, *GW* is one of the most advanced approaches yet a numerically rather expensive one [2]. A widely used alternative is density functional theory (DFT) where the speed comes at the cost of worse performance (even if there are various approaches to mitigate deficiencies, such as too small gaps) and yet faster options are available of which tight-binding approaches [3] and $k \cdot p$ models [4] will be of interest here. Such effective models need material parameters (for example on-site energies or hopping amplitudes) as an input which can sometimes be of advantage because they can be adjusted to fit experiments. Also, they may offer insight into mechanisms governing the band structure.

An archetypal example of an effective model is the Kohn-Luttinger Hamiltonian [5] which has a wide range of applications to nonmagnetic materials, including silicon and III–V semiconductors with the Γ_8 manifold at the top of the valence band (VB). Magnetism adds a new twist: for Mn-doped GaAs, the host is described by this Hamiltonian, and the effect of ferromagnetic ordering is captured by a kinetic *pd* exchange term $\propto \hat{\vec{s}} \cdot \vec{S}$ where $\hat{\vec{s}}$ is the spin operator (of the VB holes), and $\vec{S}$ is the classical spin representing the Mn magnetic moments (usually treated on the mean-field level). Such a description of ferromagnetic semiconductors [6,7] has been employed extensively in the context of spintronics [8] and now that *antiferromagnetic* spintronics [9] has become an active field, we hereby wish to contribute to its progress by presenting an effective model of hexagonal (NiAs-structure [10]) MnTe which is a well-established antiferromagnetic semiconductor as exemplified by its $T = 0$ band structure in Fig. 1 with a relatively high (≈310 K) Néel temperature. Typical samples, both bulk and epitaxial layers exhibit *p*-type conductivity, and we will, therefore, focus on its VB.

The magnetic structure of MnTe was established [11] long ago (see Fig. 3) with a strong anisotropy favoring in-plane orientation of the magnetic moments and a weak residual anisotropy within the plane [12]. Recently, Moseley *et al.* [13] have found by neutron diffraction that, upon doping by lithium, the magnetic moments rotate out of plane. They also noted that in the density of states, significant changes occur, and we use the effective model to explain how the VB responds to this change in magnetic order (once spin-orbit interaction is taken into account). Even if the Mn d states lie [14] deep below the Fermi level E_F and seem too remote from the VB top [15] which is built dominantly from p-Te orbitals, we demonstrate that the combination of the MnTe-layered structure and relativistic spin-orbit interaction (SOI) lead to an unusual sensitivity of the electronic structure to the orientation of magnetic moments. In the next section, we discuss the

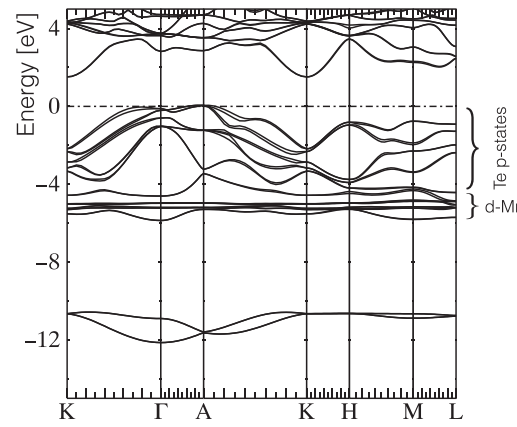

FIG. 1. Band structure of MnTe calculated by quasiparticle self-consistent *GW* (QSGW) for $\vec{L} \perp z$ (in-plane orientation). Note the competing maxima of the valence band at Γ and A points.

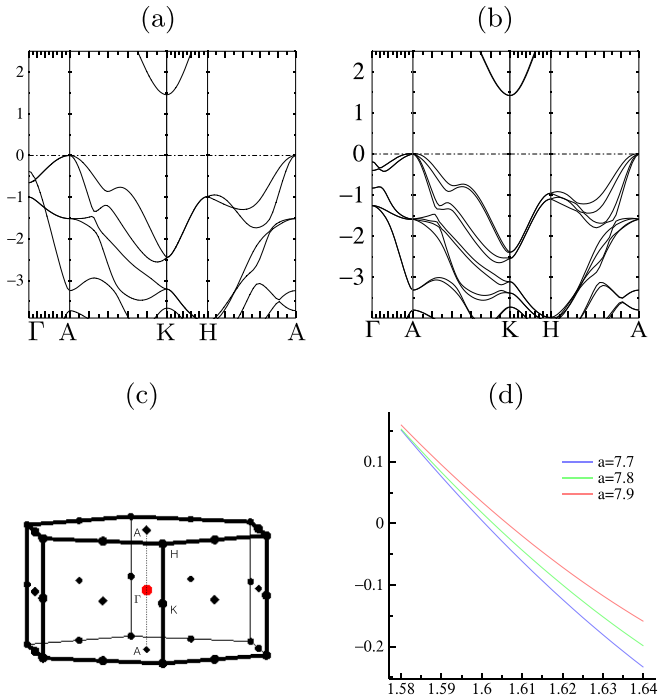

FIG. 2. Detailed view of the VB maximum and (c) the Brillouin zone of α-MnTe corresponding to lattice constants: 0.414 nm and $c/a = 1.6208$. Panels (a) and (b) show the difference between SOI ignored and included and (d) gives for the latter case the energy difference between VB maximum in Γ and A depending on the c/a ratio (for several values of a given in atomic units); origin of this dependence is discussed in Sec. 5.2 of the Supplemental Material [16]. Negative ΔE means that the VB maxima around A prevail and all energies are given in electron volt.

competing VB maxima, and we focus on the one near A point of the Brillouin zone (BZ) in Sec. III. We conclude in Sec. IV.

II. Competing VB maxima. Once the SOI is taken into account, there arises a tight competition between valence-band maxima close to A and Γ points of the BZ, see Fig. 2(b). A long-standing consensus [17,18] that the former prevails has recently been challenged by Yin *et al.* [20] who claim that the VB top occurs in the vicinity of the Γ point. To improve on the potentially less accurate DFT approach [20], we employ the quasiparticle self-consistent *GW* approximation [21]. The *GW* approximation, which is an explicit theory of

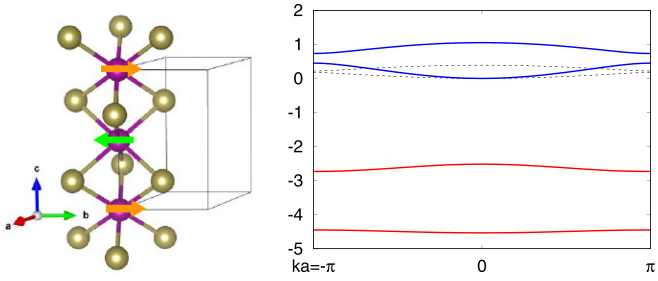

FIG. 3. NiAs structure (left) reduced to a toy model comprising a one-dimensional chain of magnetic (B) and nonmagnetic (A) atoms; there are two of the latter, A_a and A_b per unit cell. Energies are shown in the units of t and $\Delta/t = 1$, $-\epsilon_d/t = 3$ was chosen.

excited states is widely used to predict quasiparticle levels with better reliability than density functionals. QSGW is an optimized form of the *GW* approximation where the starting Hamiltonian is generated within the *GW* approximation itself, constructed so that it minimizes the difference between the one-body and the many-body Hamiltonians. As a by-product the poles of the one-body Green's function coincide with the poles of the interacting one: Thus, energy band structures have physical interpretation as quasiparticle levels, in marked contrast to DFT approaches (some examples [22,23] are given in Sec. 5.1 of the Supplemental Material [16]) where the auxillary Hamiltonian has no formal physical meaning (in practice, Lagrange multipliers of this Hamiltonian are interpreted as quasiparticle levels). It turns out that, QSGW yields high fidelity quasiparticle levels in most materials where dynamical spin fluctuations are not strong [24].

Bulk lattice constants of MnTe at room temperature are $a = 0.414$ and $c = 0.671$ nm [12]; we show in Fig. 2(d) that for such $c/a = 1.621$, the VB maximum close to the A point safely prevails (ΔE is the difference between energy of the local VB maxima close to Γ and that close to A). Most experiments nowadays are performed with thin films of MnTe, however, and then lattice constants depend on the choice of substrate. Temperature-dependent data in Fig. 3 of Ref. [12] suggest that whereas samples grown on the SrF_2 surface still fall into the same class, low temperatures may effectively push the VB maxima close to the Γ point up and, in particular, samples grown on the InP substrate may exhibit the inverted alignment of the VB maxima.

Comparing the present QSGW results to DFT calculations of Ref. [20], several remarks are in order. Lattice constants used in that reference (which correspond to $c/a = 1.57$) have been obtained by structure optimization in DFT rather than from experimental data. Next, the hybrid functional HSE06 may avoid the known problem of underestimated gaps in DFT, but this, in itself, does not guarantee a reliable description of finer details of the band structure (such as VB maxima alignment). Predicted valence and conduction bands are more uniformly reliable in *GW* than in density-functional methods. Moreover QSGW surmounts the problematic starting-point dependence that plagues the usual implementations of the *GW* approximation, and, therefore, QSGW is a better choice for our Letter than DFT. Regarding the subsequent derivation of an effective model for the VB around the Γ point [20], we note as follows. The $k_z = 0$ approximation is used; whereas this would be appropriate for very thin layers (say 5 nm), present experiments [12] are more likely behaving, such as 3D bulk. Also, the effective model (1) in Ref. [20] assumes a fixed direction of the magnetic moments; to plot the experimentally relevant "angular sweeps," the current direction rather than Néel vector is rotated which is, however, not the actual experimental protocol. For systems where only the noncrystalline anisotropic magnetoresistance (AMR) occurs [25], the two protocols are equivalent, but measurements in the Corbino geometry [12] prove this assumption false. Being aware of these issues, we strive to derive an effective model in the following which is free of these shortcomings captures the dependence on magnetic moments direction.

A proper symmetry analysis of the crystal structure of MnTe provides the nonsymmorphic space-group D^4_{6h}. Once

AF ordering is included the Mn atoms must be treated as inequivalent since each Mn layer would have spins pointing in the opposite direction as shown in Fig. 3 for in-plane spins. Hence, the symmetry group is reduced from D_{6h} to D_{3d} without SOI (see for instance Sandratskii *et al.* [26]). Furthermore, the symmetry group would also depend on the interplay of SOI and choice of the AF direction since spins pointing in different directions behave differently under symmetry operations. For example, in the out-of-plane AF configuration, the symmetry remains D_{3d} whereas for in-plane AF, either along $[10\bar{1}0]$ or $[11\bar{2}0]$ directions, the symmetry group is reduced C_{2h}. Besides the conceptual analysis of the symmetries, independent calculations using the WIEN2K and Quantum Espresso *ab initio* packages also provide the same symmetry groups discussed above. Thus, for the particular choice of in-plane AF the D_{2h} point group discussed by Yin *et al.* [20] should be replaced by C_{2h}.

III. Effective models. Several attempts to describe the electronic structure of α-MnTe in a simplified way have been made so far. Here, the $k \cdot p$ approach [4,27] is a common choice for semiconductors [28] especially if only high-symmetry points in the BZ are of interest. Such a model for the VB top in the A point was derived more than forty years ago [26] and later extended to a tight-binding scheme [29]. The latter allows for the description of the energy bands over the whole BZ but neither of these models allows to analyze the dependence of electronic structure on the directions of Mn magnetic moments. In the perfectly ordered AFM phase [as in Fig. 2(d)] and without SOI, the Bloch functions at the top of the valence band in the A point transform as the two-dimensional irreducible representation E_g or (Γ_3^+) of the D_{3d}. Including corrections up k^2 and no SOI (essentially given by Eq. (2) in Sandratskii *et al.* [26]), one would obtain the following Hamiltonian:

$$H_{kp,2\times2} = \begin{pmatrix} ak_x^2 + bk_y^2 + ck_z^2 & (a-b)k_xk_y \\ (a-b)k_xk_y & bk_x^2 + ak_y^2 + ck_z^2 \end{pmatrix}. \quad (1)$$

The inverse effective masses (proportional to a, b, and c) imply that Fermi surfaces (FSs) are, at this level of approximation, two prolate ellipsoids (one inside another and doubly degenerate) touching at the point where they are pierced by the $A\Gamma$ line; other properties of this model and its parameters, effective masses, extracted from fits to QSGW are given in Sec. 2 of the Supplemental Material [10]. From the point of view of magnetism, this is a consequence of neglecting the spin-orbit interaction. Once SOI is included, the band dispersion will depend on the direction of magnetic moments. On the other hand, if higher-order terms in $\vec{k}$ were included, the symmetry would be lowered, and FSs would become warped and spin split [30]. Consequent spin order in reciprocal space, being a hallmark [31] of so-called altermagnetism, can lead to phenomena normally unexpected in collinear compensated magnets, such as the anomalous Hall effect.

The derivation of Eq. (1) is based solely on symmetry arguments and entails neither any explicit information about orbital composition of the corresponding Bloch states nor any parametric dependence on magnetic order. In the following, we, therefore, first describe a toy model capturing the essence of interplay between magnetism and orbital degrees of freedom and next, we make use of these insights to derive a realistic model of MnTe valence band.

A. Toy model. Consider a one-dimensional chain of alternating nonmagnetic (A) and magnetic (B) atoms depicted in Fig. 3 where only the nearest neighbors couple (the amplitude being t). The single-orbital-per-site tight-binding Hamiltonian assuming that the B-atom orbitals have on-site energies $\epsilon_d \pm \Delta$ (where 2Δ is the exchange splitting) reads

$$H_1(\Delta) = \begin{pmatrix} 0 & t & 0 & te^{-ika} \\ t & \epsilon_d + \Delta & t & 0 \\ 0 & t & 0 & t \\ te^{ika} & 0 & t & \epsilon_d - \Delta \end{pmatrix}, \quad (2)$$

in the basis of Bloch states with momentum k so that ka ranging from $-\pi$ to π parametrizes the BZ.

The toy model described by H_1 can be in part treated analytically (see Ref. [16], Sec. 1) and focusing on the bands of dominantly A-atom orbital composition, we observe a downfolded cosine band of width downscaled by factor $\approx t/\epsilon_d$ in the large $|\epsilon_d|$ limit, i.e., remote B-atom dominated bands as the dashed black dispersion in Fig. 3 confirms. Atoms A_a and A_b interact only through the intermediate (magnetic) atoms B which suppresses their effective coupling. There are two main observations to make at this point. First, even if $\Delta \ll \epsilon_d$ there opens a gap in the "VB states" at the BZ edge (to make the gap better visible, we chose a larger value of Δ/ϵ_d for the blue and red bands in Fig. 3). This allows for the insight that, inasmuch the atom A_b is sandwiched between spin-up (left) and spin-down neighbors (right) where the exchange coupling is Δ and $-\Delta$, their effect on the A band (blue in Fig. 3 at the bottom right panel) does not average out to zero. Next, an even more important insight concerns the eigenstates of H_1 at $ka = \pm\pi$.

At this point, we should point out that H_1 of (2), in fact, only describes one of the two spin species; let us denote it as up-spin and, correspondingly, $H_{1,\uparrow} = H_1(\Delta)$. The two states at $ka = \pm\pi$ split by nonzero Δ turn out to be $(|a\rangle \pm |b\rangle) \otimes |\uparrow\rangle$ where $|a\rangle$ and $|b\rangle$ refer to orbitals of A_a and A_b atoms, respectively. For the spin-down sector, $H_{1,\downarrow} = H_1(-\Delta)$ which leads to identical band structure as in Fig. 3 whose eigenstates are, nevertheless, not the same as for $H_{1,\uparrow}$. The state degenerate with $(|a\rangle \pm |b\rangle) \otimes |\uparrow\rangle$ is $(|a\rangle \mp |b\rangle) \otimes |\downarrow\rangle$ and, thus, we arrive at the conclusion that at the BZ edge, the VB states in our toy model come in two pairs (split by the gap), and without loss of generality, we now focus on the subspace spanned by the pair,

$$(|a\rangle + |b\rangle) \otimes |\uparrow\rangle, \quad (|a\rangle - |b\rangle) \otimes |\downarrow\rangle. \quad (3)$$

Unlike the pair $|\uparrow\rangle, |\downarrow\rangle$ (without any orbital part), any linear combination of the two states in (3) has a zero expectation value of transversal spin operators $\hat{\sigma}_x$, $\hat{\sigma}_y$. This can also be restated as $\langle\hat{\vec{\sigma}}\rangle \| z$, or, easily generalized to the statement that the states (3) have the (expectation value of) spin parallel to the magnetic moments of atoms B. In this way, the *direction* of magnetic moments of the atoms remote in energy from the VB top influences the current-carrying states close to the Fermi energy. In the following, we denote the direction of spin in the basis state $(|a\rangle + |b\rangle) \otimes |\uparrow\rangle$, by $\vec{L}$, and it can be understood as the Néel vector. In

the following, we explore this influence in the context of spin-orbit interaction; an alternative pathway relies on spin disorder [32] (as it occurs, for example, at finite temperatures) and we outline an approach to it based on the coherent potential approximation (CPA) in the Supplemental Material [16]. It provides an alternative interpretation of "magnetic blueshift" [15] of the gap which does not rely on many-body effects.

B. Extension to the MnTe *crystal.* The previous argument can be extended to Te p_x, p_y states which form the VB top near A. To account for fine details of the band structure (as explained in Ref. [16], Sec. 2), we also include the remote p_z levels [in A, they are ≈3 eV below the VB top, see Fig. 2(a)] whose dispersion is dropped at this level of approximation. Also note that the group of VB maxima close to Γ relies on Te-p_z orbitals as explained in the Supplemental Material [10]. We will measure energy from the VB top (as it appears in the case of absent SOI) with E_F denoting the Fermi energy and use two copies of Eq. (1) to describe the $k_{x,y}$-dependent mixing of p_x, p_y orbitals. Denoting the position of p_z orbitals of tellurium by e_z ($e_z < 0$, $|e_z/E_F| \gg 1$), the full description of the VB close to A is provided by a block-diagonal 6×6 matrix,

$$H_{kp} = \begin{pmatrix} ak_x^2 + bk_y^2 + ck_z^2 & (a-b)k_xk_y & 0 & & & \\ (a-b)k_xk_y & bk_x^2 + ak_y^2 + ck_z^2 & 0 & & & \\ 0 & 0 & e_z & & & \\ & & & ak_x^2 + bk_y^2 + ck_z^2 & (a-b)k_xk_y & 0 \\ & & & (a-b)k_xk_y & bk_x^2 + ak_y^2 + ck_z^2 & 0 \\ & & & 0 & 0 & e_z \end{pmatrix}, \tag{4}$$

and the first and second 3×3 blocks are written in the basis (3) whereas inside the blocks, the basis vectors are simply $|p_x\rangle$, $|p_y\rangle$, and $|p_z\rangle$. Since the matrix (4) does not explicitly depend on $\vec{L}$ (only its basis vectors are), we arrive at the conclusion that (when SOI is ignored) the band structure does not depend on the direction of Mn magnetic moments.

In the limit $|e_z| \to \infty$, the full model (4) combined with SOI breaks down into two decoupled 2×2 blocks, and since we now have a microscopic understanding of the basis, one which contains the information about direction of Mn magnetic moments, the SOI can now be evaluated. With finite e_z, the dependence of band splitting in A can be better described as we explain in the following.

C. Spin-orbit interaction. We are now in a position to explain the following behavior of band structure calculated by relativistic *ab initio* methods. In panel (b) of Fig. 2, we could have already observed the bands split by SOI and compared to bandwidths, such splittings were small (note that these splittings cause the shift of the VB top away from A, the point of high symmetry). Those calculations were performed assuming $\vec{L} \parallel x$ and, at this level of detail, depend only little on the direction of $\vec{L}$ as long as $\vec{L} \perp z$ which is compatible with MnTe being an easy-plane material [12]. However, when $\vec{L} \parallel z$ is assumed in calculations, see Fig. 4, band splittings become sizable. Restricting our discussion to Te p_x, p_y orbitals combined into the states (3), this behavior is linked to the directionality of $H_{so} = \lambda \vec{l} \cdot \vec{\sigma}$ evaluated in the corresponding basis,

$$H_{so,2\times2} = \begin{pmatrix} 0 & i\lambda \cos\theta \\ -i\lambda \cos\theta & 0 \end{pmatrix} \tag{5}$$

where $\vec{L} \cdot \hat{z} = \cos\theta$ and $\vec{l}$ is the orbital angular momentum operator. Clearly, SOI projected to such a restricted space becomes ultimately ineffective for the in-plane orientation of magnetic moments where $\theta = \pi/2$ (taking into account also the $|p_z\rangle$ orbital in the Supplemental Material [16], small splittings at A in the in-plane configuration can, nevertheless, be also accounted for) whereas for finite e_z, the full 6×6 matrix of H_{so} must be considered instead of (5). On the other hand, for out-of-plane magnetic moments, the splitting at A seen in Fig. 4 can be directly compared to eigenvalues $\pm\lambda$ of $H_{so,2\times2}$.

IV. Discussion and conclusions. An effective model of the MnTe valence band around A point of the BZ depends on the level of detail needed: Eq. (1) is a meaningful approximation to begin with, but it cannot describe the band-dispersion dependence on the direction of Mn magnetic moments and spin splitting in Fig. 2(b); the six-band (or four-band, corresponding to the $|e_z| \to \infty$ limit) description using Eq. (4) combined with H_{so} evaluated with respect to basis (3) times $|p_x\rangle$, $|p_y\rangle$, and $|p_z\rangle$ is the reasonable next step. On this level, the large sensitivity of the valence band at A to magnetic moment orientation can be explained in terms of zero matrix elements of H_{so} between $(|a\rangle + |b\rangle) \otimes |{\rightarrow}\rangle$ and $(|a\rangle - |b\rangle) \otimes |{\leftarrow}\rangle$ where a, b refer to the two Te atoms within the unit cell

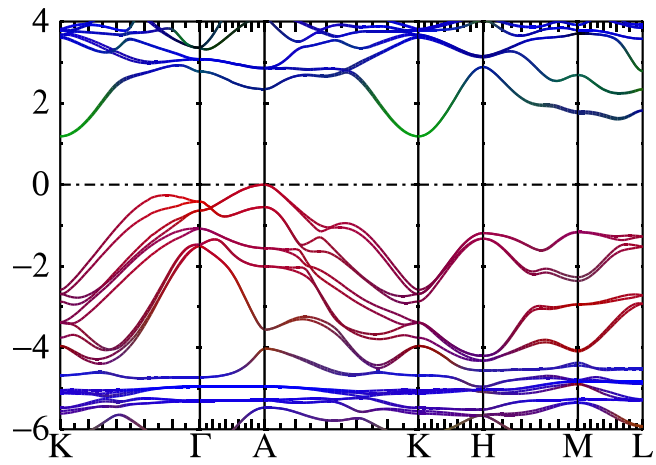

FIG. 4. MnTe band structure for $\vec{L} \parallel z$ (energies in eV). Color coding: red: Te; blue: Mn.

of MnTe. Zooming into the details of the valence band smaller than ∼100 meV would require adding further terms, such as those discussed on p. 8 of the Supplemental Material to Ref. [30]; on this level of approximation, phenomena, such as the anomalous Hall effect or AMR can then likely be successfully modeled.

Calculations in Fig. 4 show that the splitting at A is associated with reduction of the band gap in agreement with DFT calculations [13]. This implies that not only angular-resolved photoemission could be used to confirm the sensitivity of the MnTe band structure to the orientation of Mn magnetic moments, but also optical absorption measurements should reveal signatures of this effect. Such experiments could also confirm our results concerning the competition of valence-band maxima close to the A and Γ points of the Brillouin zone.

Acknowledgments. We acknowledge assistance of Swagata Acharya with QSGW calculations and a preliminary KKR survey by A. Marmodoro; funding was provided by Grants No. 22-21974S and EU FET Open RIA No. 766566, M.v.S. was supported by the DOE-BES Division of Chemical Sciences under Contract No. DE-AC36-08GO28308 and P.E.F.J. acknowledges financial support from the Alexander von Humboldt Foundation, Capes (Grant No. 99999.000420/2016-06) and Deutsche Forschungsgemeinschaft SFB 1277 (Project No. ID314695032, Subprojects No. B07 and No. B11).

[1] F. Tran, J. Doumont, L. Kalantari, A. W. Huran, M. A. L. Marques, and P. Blaha, J. Appl. Phys. **126**, 110902 (2019).
[2] M. Grumet, P. Liu, M. Kaltak, J. Klimeš, and G. Kresse, Phys. Rev. B **98**, 155143 (2018).
[3] O. K. Andersen and O. Jepsen, Phys. Rev. Lett. **53**, 2571 (1984).
[4] R. Winkler, *Spin-orbit Coupling Effects in Two-Dimensional Electron and Hole Systems* (Springer, New York, 2003).
[5] J. M. Luttinger, Phys. Rev. **102**, 1030 (1956).
[6] M. Tanaka, Jpn. J. Appl. Phys. **60**, 010101 (2021).
[7] T. Jungwirth, J. Wunderlich, V. Novák, K. Olejník, B. L. Gallagher, R. P. Campion, K. W. Edmonds, A. W. Rushforth, A. J. Ferguson, and P. Němec, Rev. Mod. Phys. **86**, 855 (2014).
[8] C. H. Marrows and B. J. Hickey, Philos. Trans. R. Soc. A. **369**, 3027 (2011).
[9] V. Baltz, A. Manchon, M. Tsoi, T. Moriyama, T. Ono, and Y. Tserkovnyak, Rev. Mod. Phys. **90**, 015005 (2018).
[10] K. Adachi, J. Phys. Soc. Jap. **16**, 2187 (1961) and references therein; apart from the NiAs-type structure of MnTe, zinc-blende phase also exists which is AFM at low temperatures.
[11] T. Komatsubara, M. Murakami, and E. Hirahara, J. Phys. Soc. Jpn. **18**, 356 (1963).
[12] D. Kriegner, H. Reichlová, J. Grenzer, W. Schmidt, E. Ressouche, J. Godiñho, T. Wagner, S. Y. Martin, A. B. Shick, V. V. Volobuev *et al.*, Phys. Rev. B **96**, 214418 (2017).
[13] D. H. Moseley, K. M. Taddei, J. Yan, M. A. McGuire, S. Calder, M. M. H. Polash, D. Vashaee, X. Zhang, H. Zhao, D. S. Parker *et al.*, Phys. Rev. Mater. **6**, 014404 (2022).
[14] H. Sato, M. Tamura, N. Happo, T. Mihara, M. Taniguchi, T. Mizokawa, A. Fujimori, and Y. Ueda, Solid State Commun. **92**, 921 (1994).
[15] D. Bossini, M. Terschanski, F. Mertens, G. Springholz, A. Bonanni, G. S. Uhrig, and M. Cinchetti, New J. Phys. **22**, 083029 (2020).
[16] See Supplemental Material at http://link.aps.org/supplemental/10.1103/PhysRevB.107.L100417 for details of the effective model including its parameters, CPA treatment of the toy model, and comparison between DFT methods.
[17] M. Podgorny and J. Oleszkiewicz, J. Phys. C: Sol. St. Phys. **16**, 2547 (1983).
[18] More recent studies range from S. J. Youn, B. I. Min, and A. J. Freeman, Phys. Status Solidi B **241**, 1411 (2004); to Mu *et al.* [19] and this VB maxima alignment is also consistent with our previous DFT $+U$ calculations [12].
[19] S. Mu, R. P. Hermann, S. Gorsse, H. Zhao, M. E. Manley, R. S. Fishman, and L. Lindsay, Phys. Rev. Mater. **3**, 025403 (2019).
[20] G. Yin, J.-X. Yu, Y. Liu, R. K. Lake, J. Zang, and K. L. Wang, Phys. Rev. Lett. **122**, 106602 (2019).
[21] T. Kotani, M. van Schilfgaarde, and S. V. Faleev, Phys. Rev. B **76**, 165106 (2007).
[22] M. Krause and F. Bechstedt, J. Supercond. Nov. Magn. **26**, 1963 (2013).
[23] F. Tran and P. Blaha, Phys. Rev. B **83**, 235118 (2011).
[24] M. van Schilfgaarde, T. Kotani, and S. Faleev, Phys. Rev. Lett. **96**, 226402 (2006).
[25] A. W. Rushforth, K. Výborný, C. S. King, K. W. Edmonds, R. P. Campion, C. T. Foxon, J. Wunderlich, A. C. Irvine, P. Vašek, V. Novák, K. Olejník, J. Sinova, T. Jungwirth, and B. L. Gallagher, Phys. Rev. Lett. **99**, 147207 (2007); P. Ritzinger and K. Vyborny, arXiv:2212.03700.
[26] L. M. Sandratskii, R. F. Egorov, and A. A. Berdyshev, Phys. Status Solidi B **104**, 103 (1981).
[27] L. C. Lew Yan Voon and M. Willatzen, *The k · p Method: Electronic Properties of Semiconductors* (Springer, Berlin, 2009).
[28] P. E. Faria Junior, T. Campos, C. M. O. Bastos, M. Gmitra, J. Fabian, and G. M. Sipahi, Phys. Rev. B **93**, 235204 (2016).
[29] J. Mašek, B. Velický, and V. Janiš, J. Phys. C: Solid State Phys. **20**, 59 (1987).
[30] L. Šmejkal, J. Sinova, and T. Jungwirth, Phys. Rev. X **12**, 031042 (2022).
[31] L. Šmejkal, J. Sinova, and T. Jungwirth, Phys. Rev. X **12**, 040501 (2022); I. Turek, Phys. Rev. B **106**, 094432 (2022).
[32] R. Baral, J. A. Christensen, P. K. Hamilton, F. Ye, K. Chesnel, T. D. Sparks, R. Ward, J. Yan, M. A. McGuire, M. E. Manley *et al.*, Matter **5**, 1853 (2022).